A Simple Mixed-Based Approach for Thin-Walled Composite Blades with Two-Cell Sections

Sung Nam Jung* Il-Ju Park
School of Mechanical and Aerospace Engineering,
Chonbuk National University, Jeonju 561-756, Korea

In this work, a mixed beam approach that combines both the stiffness and the flexibility methods has been performed to analyze the coupled composite blades with closed, two-cell cross-sections. The Reissner's semi-complementary energy functional is used to derive the beam force-displacement relations. Only the membrane part of the shell wall is taken into account to make the analysis simple and also to deliver a clear picture of the mixed method. All the cross-section stiffness coefficients as well as the distribution of shear across the section are evaluated in a closed-form through the beam formulation. The theory is validated against experimental test data, detailed finite element analysis results, and other analytical results for coupled composite blades with a two-cell airfoil section. Despite the simple kinematic model adopted in the theory, an accuracy comparable to that of two-dimensional finite element analysis has been obtained for cases considered in this study.

Key Words : Mixed Beam Approach, Coupled Composite Blades, Two-cell Airfoil Section, Closed-form Solution

1. Introduction

In general, the composite rotor blades are built-up structures made of different materials for the skin and spar and are normally of closed single- or multi-celled cross-sections and are thin-walled except near the root where they become thick-walled. In the analysis of composite blades, there is a need to properly model the local behavior of the shell wall as a reaction to the global deformation of the blade (Jung et al., 1999).

During last couple of decades, a few selected research activities have been devoted to model and analyze elastically-coupled composite beams and blades with multi-cell sections (Mansfield, 1981 ; Chandra and Chopra, 1992 ; Volovoi and Hodges, 2002 ; Badir, 1995 ; Jung and Park, 2005). Most of the beam approaches found in the literature have been formulated through either a displacement (Smith and Chopra, 1991 ; Chandra and Chopra, 1992; Song and Librescu, 1997; Shim and Na, 2003) or a force method (Mansfield, 1981 ; Libove, 1988). The former is based on a suitable approximation to the displacement field of the shell wall of the section. The assumed displacement field is used to compute the strain energy of the beam, and the beam stiffness relations are obtained by introducing relevant energy principles. The stiffness method is quite straightforward and easy to apply but there is no systematic method to determine the distribution of warpings that can be an important factor in enhancing the accuracy of the analysis particularly for thin-walled blades. While, in the force method, also called the flexibility formulation, the assumed direct stress field in the shell wall is used to obtain the distribution of the shear stress and the associated warpings directly from the equilibrium equations of the shell wall. The flexibility method provides a sys-

* Corresponding Author,
E-mail : snjung@chonbuk.ac.kr
TEL : +82-63-270-2469; **FAX** : +82-63-270-2472
School of Mechanical and Aerospace Engineering, Chonbuk National University, Jeonju 561-756, Korea.
(Manuscript **Received** April 20, 2005; **Revised** September 21, 2005)

tematic method to determine the warping functions and generally leads to better correlation with experimental test data.

Recently, the mixed method that combines both the displacement and force methods effectively by using the variational-asymptotic framework (Volovoi and Hodges, 2002; Badir, 1995) or the Reissner's functional (Jung and Park, 2005) has been reported in the literature. These newly developed beam theories allow treatment of arbitrary cross-section geometries and material distributions. The bending shell strain measures as well as the membrane shell strains are incorporated in these approaches to take into account the wall thickness effect of the beam section. It has been shown that the mixed theories are generic and accurate enough for the analysis of elastically-coupled, thin-walled composite blades. Even though more rigorous representation of beam kinematics is truly desirable for refined analysis, a simple but generic approach that can give us a physical insight into the complex coupling mechanism is needed as a way to improve the basic understanding of composites necessary in the design of a composite blade.

In the present work, a simple approach based on a mixed method is proposed by taking into account the membrane shell of the section wall toward modeling and analyzing the thin-walled composite blades with two-cell sections. A closed-form expression is obtained for the cross-section stiffness coefficients as well as the distribution of shear across the section. The theory is validated by comparison of the static response of coupled composite blades with experimental results found in the literature and also with those of a detailed finite element analysis using the MSC/NASTRAN.

2. Formulation

Figure 1 shows the geometry and coordinates of a thin-walled composite blade with two-cell airfoil section. Two different systems of coordinate axes are used: an orthogonal Cartesian coordinate system (x, y, z) for the blade, where x is the reference axis of the blade and y and z are the transverse coordinates of the cross section; a curvilinear coordinate system (x, s, n) for the shell wall of the section, where s is a contour coordinate measured along the middle surface of the shell wall and n is normal to this contour coordinate. The global deformations of the beam are (U, V, W) along the x, y and z axes, and ϕ is the elastic twist about the x-axis. The mid-plane (contour) shell deformations are (u^0, v_t^0, v_n^0) along the x, s and n directions, respectively. From a geometric consideration as depicted in Fig. 2, the mid-plane shell displacements can be obtained in terms of the beam displacements and

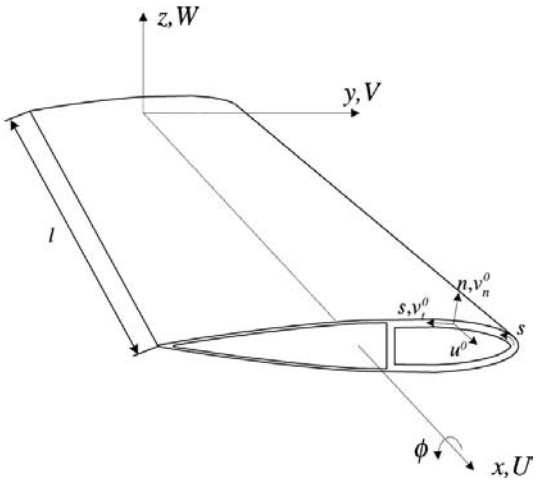

Fig. 1 Geometry and coordinate systems of a two-cell blade

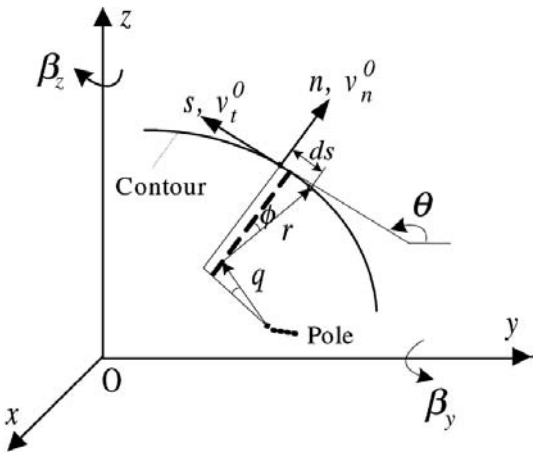

Fig. 2 Coordinates and sign convention

rotations :

$$v_t^0 = Vy,_s + Wz,_s + r\phi$$
$$v_n^0 = Vz,_s - Wy,_s - q\phi \quad (1)$$

where the superscript 0 denotes that the value is defined at the midplane contour of the shell wall and r and q are the coordinates of an arbitrary point on the shell wall in the (n, s) coordinate system (see Fig. 2), and the comma refers to the derivative with respect to the coordinate. Based on a small strain assumption, the membrane shell strain measures are given by :

$$\varepsilon_{xx} = u,_x^0$$
$$\gamma_{xs} = u,_s^0 + v,_x^0 \quad (2)$$

By substituting Eq. (1) into the shear strain γ_{xs} in Eq. (2) and integrating this partially with respect to x, the following relation is obtained,

$$\gamma_{xs} = u,_s^0 + V,_x y,_s + W,_x z,_s + r\phi,_x \quad (3)$$

From the geometric relationships depicted in Fig. 2, the shell shear strain γ_{xs} can also be written in terms of the shear strains in the Cartesian system of coordinates,

$$\gamma_{xs} = \gamma_{xy} \cos\theta + \gamma_{xz} \sin\theta = \gamma_{xy} y,_s + \gamma_{xz} z,_s \quad (4)$$

where θ is the angle between the positive x and s directions (see Fig. 2), and γ_{xy} and γ_{xz} represent the transverse shear strains of the blade and are related to the cross-section rotations β_y and β_z about the y and z axes, respectively, as :

$$\beta_y = \gamma_{xz} - W,_x$$
$$\beta_z = \gamma_{xy} - V,_x \quad (5)$$

The positive direction for the section rotations is defined in Fig. 2. By equating Eqs. (3) and (4) and integrating with the contour coordinate s, the axial strain can be obtained in terms of the beam displacement derivatives :

$$\varepsilon_{xx} = U,_x + z\beta_{y,x} + y\beta_{z,x} - \bar{\omega}\phi,_{xx} \quad (6)$$

where $\bar{\omega}$ is the sectorial area of the section (Gjelsvik, 1981). The strain-displacement relation of Eq. (6) forms the basis of the displacement method for thin-walled blades.

Assuming the hoop stress flow N_{ss} is negligibly small, the constitutive relations for the shell wall of the section can be written as

$$\begin{Bmatrix} N_{xx} \\ N_{xs} \end{Bmatrix} = \begin{bmatrix} A'_{11} & A'_{16} \\ A'_{16} & A'_{66} \end{bmatrix} \begin{Bmatrix} \varepsilon_{xx} \\ \gamma_{xs} \end{Bmatrix} \quad (7)$$

with

$$A'_{11} = A_{11} - \frac{A_{12}^2}{A_{22}}$$
$$A'_{16} = A_{16} - \frac{A_{12}A_{26}}{A_{22}} \quad (7a)$$
$$A'_{66} = A_{66} - \frac{A_{26}^2}{A_{22}}$$

where A_{ij} are the laminate stiffness coefficients in the classical lamination theory (Jones, 1975). Note that only the membrane action of the shell wall is considered in the above constitutive relations. In case where the bending strain measures become important, these should also be incorporated in the analysis (Jung et al., 2002). It is convenient to write Eq. (7) in a semi-inverted form as :

$$\begin{Bmatrix} N_{xx} \\ \gamma_{xs} \end{Bmatrix} = \begin{bmatrix} A_{n\varepsilon} & A_{n\gamma} \\ -A_{n\gamma} & A_{\gamma\gamma} \end{bmatrix} \begin{Bmatrix} \varepsilon_{xx} \\ N_{xs} \end{Bmatrix} \quad (8)$$

where

$$A_{n\varepsilon} = A'_{11} - \frac{A'^2_{16}}{A'_{66}},\ A_{n\gamma} = \frac{A'_{16}}{A'_{66}},\ A_{\gamma\gamma} = \frac{1}{A'_{66}} \quad (8a)$$

In order to assess the semi-inverted constitutive relations into the beam formulation, a modified form of Reissner's semi-complimentary energy functional Φ_R is introduced (Murakami et al., 1996):

$$\Phi_R = \frac{1}{2}[N_{xx}\varepsilon_{xx} - \gamma_{xs}N_{xs}] \quad (9)$$

The stiffness matrix relating beam forces to beam displacements is obtained by using the variational statement of the Reissner functional which is given by

$$\delta \int_0^l \oint_C (\Phi_R + \gamma_{xs}N_{xs})\, ds dx = 0 \quad (10)$$

where l is the length of the blade and C is the contour of the closed section. The parenthesis of Eq. (10) represents the strain energy density of the blade. As is expected from Eq. (8), the shear flow N_{xs} is treated as an unknown variable unlike the displacement-based approach, while the axial strain is treated as the known. The shear flow N_{xs}

is determined from the continuity condition of the axial displacement of the shell wall which is written as :

$$\int_C u^0_{,s}\, ds = 0 \tag{11}$$

The shear strain can be rewritten by using Eqs. (3) and (8) as :

$$\begin{aligned}\gamma_{xs} &= -A_{n\gamma}\varepsilon_{xx} + A_{\gamma\gamma}N_{xs} \\ &= u^0_{,s} + V_{,x}y_{,s} + W_{,x}z_{,s} + r\phi_{,x}\end{aligned} \tag{12}$$

Integrating Eq. (12) from 0 to s and invoking the continuity condition (Eq. (11)) for each wall of the section, one can obtain the following equations

$$\begin{aligned}(\alpha_1+\alpha_3)\, n_I - \alpha_3 n_{II} &= 2A_I\phi_{,x} + \int_{C_1+C_3} A_{n\gamma}\varepsilon_{xx}ds \\ -\alpha_3 n_I + (\alpha_2+\alpha_3)\, n_{II} &= 2A_{II}\phi_{,x} + \int_{C_2+C_3} A_{n\gamma}\varepsilon_{xx}ds\end{aligned} \tag{13}$$

where n_I and n_{II} are unknown shear flows for each cell of the section, A_I and A_{II} are enclosed areas of the two cells, and C_i $(i=1, 2, 3)$ are the contour lengths of the section segments (see Fig. 3). Considering the geometry in Fig. 3, the shear flow components corresponding to each of the three curves C_1, C_2, and C_3 lead to n_I, n_{II} and $n_I - n_{II}$, respectively. The α_1, α_2, and α_3 appeared in Eq. (13) are defined as

$$\alpha_1 = \int_{C_1} A_{\gamma\gamma}ds\ ;\ \alpha_2 = \int_{C_2} A_{\gamma\gamma}ds\ ;\ \alpha_3 = \int_{C_3} A_{\gamma\gamma}ds \tag{14}$$

By substituting the axial strain Eq. (6) into Eq. (13), the unknown shear flows are determined as

$$\{n\} = [f]\{q_b\} \tag{15}$$

where

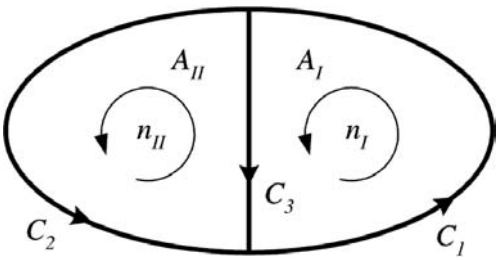

Fig. 3 Definition of a two-cell section

$$\{n\} = \lfloor n_I\ n_{II} \rfloor^T$$

$$[f] = \begin{bmatrix} f_{x1} & f_{y1} & f_{z1} & f_{\phi 1} & f_{\omega 1} \\ f_{x2} & f_{y2} & f_{z2} & f_{\phi 2} & f_{\omega 2} \end{bmatrix} \tag{16}$$

$$\{\bar{q}_b\} = \lfloor U_{,x}\ \beta_{y,x}\ \beta_{z,x}\ \phi_{,x}\ \phi_{,xx} \rfloor^T$$

where the superscript T denotes the transpose of a vector. The components of $[f]$ in Eq. (16) are given in Appendix (Eqs. (a1)~(a2)).

Inserting Eqs. (3) and (13) into Eq. (9) and using Eq. (15), one can obtain the following set of beam forces-displacements relations,

$$\{F_b\} = \lfloor N\ M_y\ M_z\ T\ M_\omega \rfloor^T = [K_{bb}]\{q_b\} \tag{17}$$

where N is the axial force, M_y and M_z are bending moments about y and z directions, respectively, T is the twisting moment and M_ω is the Vlasov bi-moment. The cross-section stiffness matrix $[K_{bb}]$ relates the cross-section force and moment resultants with beam displacements in an Euler-Bernoulli level of approximation for extension and bending and Vlasov level for torsion. The elements of $[K_{bb}]$ for thin-walled blades with a two-celled section are obtained in a closed-form as in Eq. (a4).

3. Results and Discussions

Numerical investigation has been performed to validate the current analysis with available literature. Thin-walled, two-cell composite blades with extension-torsion or bending-torsion couplings are considered in this study. Fig. 4 shows the schematic of the two-cell blade section fabricated and tested by Chandra and Chopra (1991, 1992). The section has a NACA 0012 contour and consists of D-shape spar, web and skin. The blade is clamped at one end and warping restrained at both ends. The geometry and the material properties of the blade are given in Table 1.

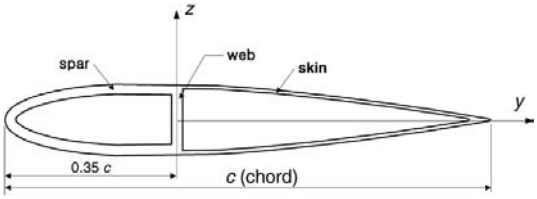

Fig. 4 Schematic of a two-cell airfoil section

Blades with six different layup cases representing extension-torsion (Blade 1 to 3) or bending-torsion (Blade 4 to 6) couplings are examined. Table 2 shows the details of the layup for the cases. The positive fiber angle is defined as having a right angle with respect to the outward normal vector n along the contour of the section wall (see Fig. 1).

Figure 5 shows the comparison results of the tip bending slopes for the extension-torsion coupled blades (Blade 1 to 3) subjected to a unit tip shear load. As is seen in Table 2, Blades 1 to 3 consist of $[0/\theta]_2$ spar, $[0/\theta]_2$ web and $[\theta/-\theta]$ skin where the ply angles are varied from 15 (Blade 1), 30 (Blade 2) and 45 (Blade 3) degrees. The present predictions are compared with the experimental test data and the theoretical results obtained by Chandra and Chopra (1992) along with those of the two-dimensional MSC/NASTRAN analysis. For the NASTRAN results, a total of 15,800 CQUAD4 plate/shell finite elements leading 77,721 degrees of freedom are used. The finite element meshes used for the NASTRAN analysis are presented in Fig. 6 for a reference purpose. For the present results, the contour in the rear and front cells of the NACA 0012 section is divided into 100 and 800 linear segments, respectively, only to perform the contour integrals numerically for the section. As can be seen in Fig. 5, the predictions obtained by the present method are in excellent agreements with experimental test data as well as with the MSC/NASTRAN results. The error between the present results and the experimental test data is within 4.3% for all the cases. The variance between the current predictions and those of Chandra and Chopra (1992) is thought to be due to the differences in the constitutive relations adopted in the two theories : The current approach used the

Table 1 Geometry and material properties of graphite-epoxy blades

E_{11}	131 GPa (19×10^6 psi)
E_{22}	9.3 GPa (1.35×10^6 psi)
G_{12}	5.36 GPa (0.85×10^6 psi)
ν_{12}	0.40
Ply thickness	0.127 mm (0.005 in)
Airfoil	NACA 0012
Length	641.4 mm (25.25 in)
Chord	76.2 mm (3 in)
Airfoil thickness	9.144 mm (0.36 in)

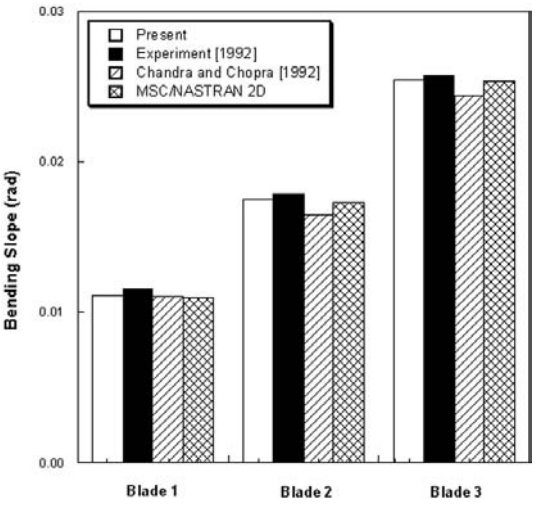

Fig. 5 Comparison of tip bending slopes for extension-torsion coupled blades under unit a tip shear load

Table 2 Layup cases of elastically-coupled composite blades

	Cases	Spar		Web	Skin
		Top Flange	Bottom Flange		
Extension-Torsion Coupled Blades	Blade 1	$[0/15]_2$	$[0/15]_2$	$[0/15]_2$	$[15/-15]$
	Blade 2	$[0/30]_2$	$[0/30]_2$	$[0/30]_2$	$[30/-30]$
	Blade 3	$[0/45]_2$	$[0/45]_2$	$[0/45]_2$	$[45/-45]$
Bending-Torsion Coupled Blades	Blade 4	$[0/15]_4$	$[0/-15]_4$	$[0/\pm15/0]_2$	$[15/-15]$
	Blade 5	$[0/30]_4$	$[0/-30]_4$	$[0/\pm30/0]_2$	$[30/-30]$
	Blade 6	$[0/45]_4$	$[0/-45]_4$	$[0/\pm45/0]_2$	$[45/-45]$

zero hoop-stress-flow assumption ($N_{ss}=0$) while a zero in-plane-strain assumption ($\gamma_{ss}=\kappa_{ss}=0$) was used in their approach (Chandra and Chopra, 1992). It should be noted that the bending shell strain measure as well as the membrane strain are incorporated in the theory (Chandra and Chopra, 1992) whereas only the membrane shell measure is included in the present analysis. The result indicates that, despite a simple model, accurate analysis results are obtained with the present mixed method.

Figure 7 presents the tip twist results obtained respectively for Blades 1 to 3 under a unit tip torque load. A good correlation with experimental results is clearly seen in the figure. For this case, the errors are within 4.7% for the direct tip twist response.

Figures. 8~9 show the comparison results of both the tip bending slope and the induced tip twist response, respectively, for the bending-tor-

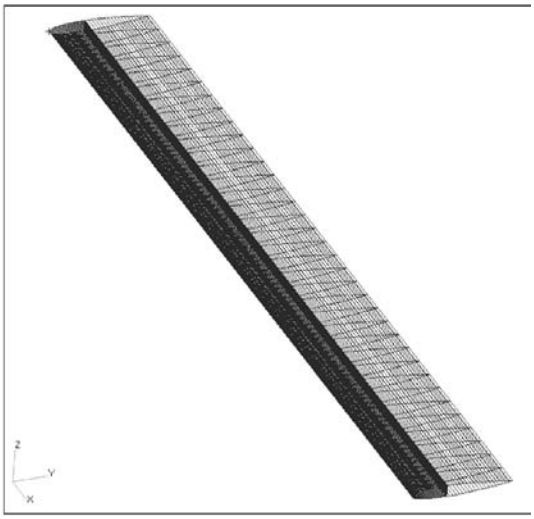

Fig. 6 Two-dimensional meshes for the MSC/NASTRAN analysis

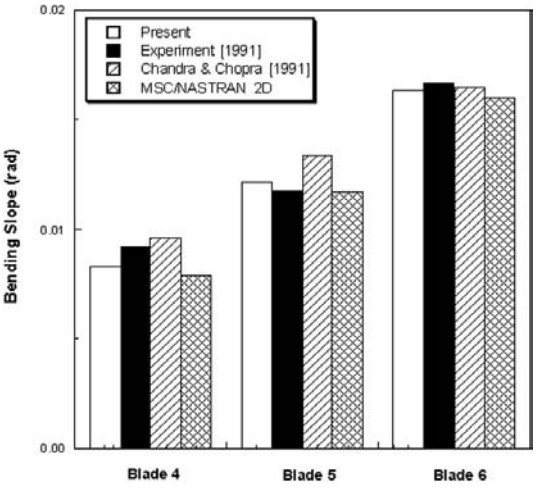

Fig. 8 Comparison of tip bending slopes for bending-torsion coupled blades under unit a tip shear load

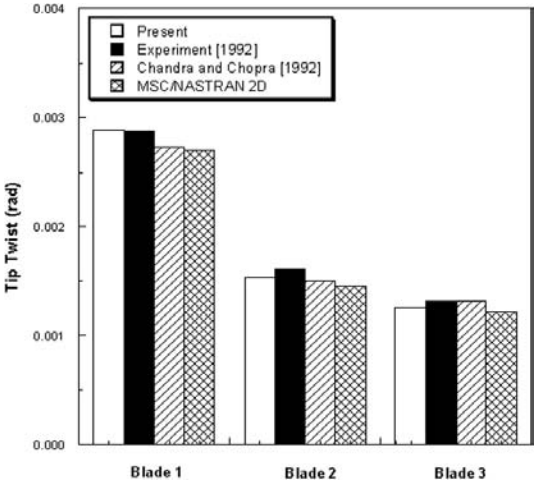

Fig. 7 Comparison of tip twist angles for extension-torsion coupled blades under a unit tip torque load

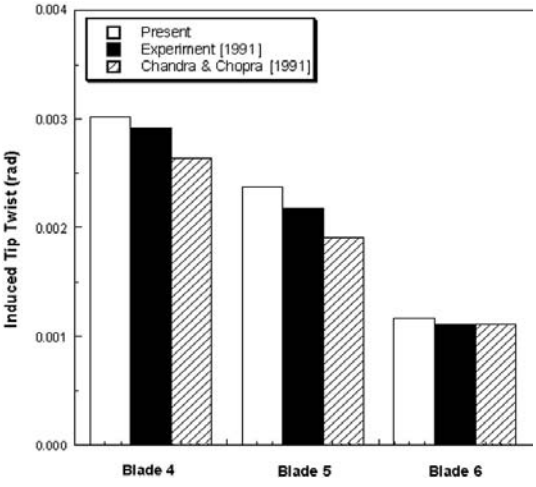

Fig. 9 Comparison of induced twist angles for bending-torsion coupled blades under a unit tip shear load

sion coupled blades (Blade 4 to 6) which are subjected to a unit tip shear load. The details of the layup for Blades 4 to 6 are given in Table 2. In this case, the non-zero ply angles used in the top and bottom flanges of the spar result in a bending-torsion coupling while the layups in both the web and skin produce no elastic couplings. The twist deformation is induced because of the bending-torsion couplings when the load is applied at the tip of the blades. As can be seen from Figs. 8~9, the present results are in good agreements with experimental test data. The error is less than 10% for the direct bending response (Fig. 8) and 8.8% for the bending-induced twist response (Fig. 9). It is observed that the results obtained by the present method present better correlations with the experimental results than those obtained by Chandra and Chopra (1991). One thing to be addressed in Fig. 9 that the current predictions show a softening behavior compared to the experimental test data. This trend seems obvious with a view of the fact that the current theory takes into account the thickness effect of the shell wall as a membrane shell that actually leads to a more flexible representation of the structure. In some cases where the thickness effects of the shell wall become more important, the bending shell strain measure as well as the membrane measure should be incorporated in the analysis. As mentioned in the Introduction section, however, this can make the theory more involved and complex to an unacceptable and unrealistic level.

Figures 10~11 show the comparison results of the direct tip twist response as well as the torsion-induced bending response for Blades 4 to 6 undergoing a unit tip torque load. The correlation with experimental results is good for the direct twist response (Fig. 10) and fair for the induced response (Fig. 11). A large variation between the three different set of approaches is noticed especially for Blade 5 case in the induced response (Fig. 11). For this specific case, the error between the current predictions and the experimental results is about 15%. A refined experimental test along with a more sophisticated loading and clamping mechanism seems necessary to enhance the correlation between the results. As in the previous case, a slightly better correlation with experimental results is observed in comparison with the predictions obtained by Chandra and Chopra (1991).

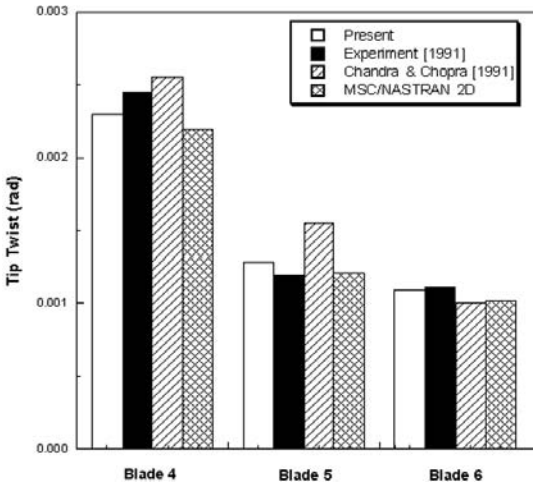

Fig. 10 Comparison of tip twist angles for bending-torsion coupled blades under unit a tip torque load

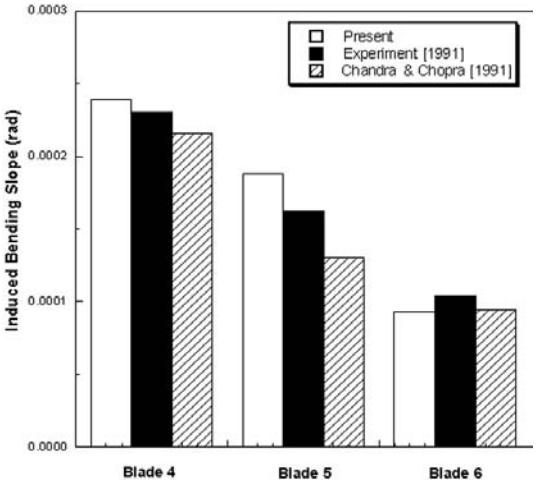

Fig. 11 Comparison of induced tip bending slopes for bending-torsion coupled blades under a unit tip torque load

4. Concluding Remarks

In the present work, a closed-form analysis for coupled composite blades with multiple cell sec-

tions was performed. The analysis model included the effects of elastic couplings, shell wall thickness, torsion warping and constrained warping. The beam force-displacement relations of the blade were obtained by using the Reissner's semi-complementary energy functional. All the cross-section stiffness coefficients as well as the distribution of shear across the section were obtained in a closed-form through the beam formulation. The theory was correlated with experimental test data, other theoretical results and detailed finite element results for bending-torsion or extension-torsion coupled composite blades with a two-cell airfoil section. In general, good correlation of responses with experimental results was obtained for the cases considered in this study. The error was generally less than 5% for blades with extension-torsion couplings and 15% with bending-torsion couplings.

References

Badir, A.M, 1995, "Analysis of Two-Cell Composite Beams," *Proceedings of the 36th Structures, Structural Dynamics, and Materials Conference*, New Orleans, LA, Apr. 10-12, pp. 419～424.

Chandra, R. and Chopra, I., 1991, "Coupled Composite Rotor Blades under Bending and Torsional Loads," *AHS Specialist Meeting on Rotorcraft Structures*, Williamsburg, VA, Oct. 28-31.

Chandra, R. and Chopra, I., 1992, "Structural Behavior of Two-Cell Composite Rotor Blades with Elastic Couplings," *AIAA Journal*, Vol. 30, No. 12, pp. 2914～2921.

Gjelsvik, A., 1981, *The Theory of Thin Walled Bars*, John Wiley & Sons, Inc..

Jung, S. N., Nagaraj, V. T. and Chopra, I., 1999, "Assessment of Composite Rotor Blade Modeling Techniques," *Journal of the American Helicopter Society*, Vol. 44, No. 3, pp. 188～205.

Jung, S. N., Nagaraj, V. T. and Chopra, I., 2002, "Refined Structural Model for Thin- and Thick-Walled Composite Rotor Blades," *AIAA Journal*, Vol. 40, No. 1, pp. 105～116.

Jung, S. N. and Park, I. J., 2005, "Structural Behavior of Thin- and Thick-Walled Composite Blades with Multicell Sections," *AIAA Journal*, Vol. 43, No. 3, pp. 572～581.

Jones, R. M., 1975, *Mechanics of Composite Materials*, McGraw-Hill Book Co., N.Y..

Libove, C., 1988, "Stress and Rate of Twist in Single-Cell Thin-Walled Beams with Anisotropic Walls," *AIAA Journal*, Vol. 26, No. 9, pp. 1107～1118.

Mansfield, E. H., 1981, "The Stiffness of a Two-Cell Anisotropic Tube," *Aeronautical Quarterly*, pp. 338～353.

Murakami, H., Reissner, E., and Yamakawa, J., 1996, "Anisotropic Beam Theories with Shear Deformation," *Journal of Applied Mechanics*, Vol. 63, No. 3, pp. 660～668.

Smith, E. C. and Chopra, I, 1991, "Formulation and Evaluation of an Analytical Model for Composite Box-Beams," *Journal of the American Helicopter Society*, Vol. 36, No. 3, pp. 23～35.

Song, O. and Librescu, L., 1997, "Structural Modeling and Free Vibration Analysis of Rotating Composite Thin-Walled Beams," *Journal of the American Helicopter Society*, Vol. 42, No. 4, pp. 358～369.

Shim, J. K. and Na, S., 2003, "Modeling and Vibration Feedback Control of Rotating Tapered Composite Thin-Walled Blade," *KSME Int. Journal*, Vol. 17, No. 3, pp. 380～390.

Volovoi, V. V. and Hodges, D. H., 2002, "Single- and Multicelled Composite Thin-Walled Beams," *AIAA Journal*, Vol. 40, No. 5, pp. 960～965.

Appendix

The shear flow components appeared in Eq. (16) are given by:

$$f_{x1}=\{(\alpha_2+\alpha_3)\int_{C_1+C_3}A_{n\gamma}ds+\alpha_3\int_{C_2+C_3}A_{n\gamma}ds\}/\Delta$$

$$f_{y1}=\{(\alpha_2+\alpha_3)\int_{C_1+C_3}A_{n\gamma}zds+\alpha_3\int_{C_2+C_3}A_{n\gamma}zds\}/\Delta$$

$$f_{z1}=\{(\alpha_2+\alpha_3)\int_{C_1+C_3}A_{n\gamma}yds+\alpha_3\int_{C_2+C_3}A_{n\gamma}yds\}/\Delta \quad \text{(a1)}$$

$$f_{\phi 1}=\{(\alpha_2+\alpha_3)\cdot 2A_I+\alpha_3\cdot 2A_{II}\}/\Delta$$

$$f_{\omega 1}=-\{(\alpha_2+\alpha_3)\int_{C_1+C_3}A_{n\gamma}\bar{\omega}ds+\alpha_3\int_{C_2+C_3}A_{n\gamma}\bar{\omega}ds\}/\Delta$$

$$f_{x2}=\{\alpha_3\int_{C_1+C_3}A_{n\gamma}ds+(\alpha_1+\alpha_3)\int_{C_2+C_3}A_{n\gamma}ds\}/\Delta$$

$$f_{y2}=\{\alpha_3\int_{C_1+C_3}A_{n\gamma}zds+(\alpha_1+\alpha_3)\int_{C_2+C_3}A_{n\gamma}zds\}/\Delta \quad \text{(a2)}$$

$$f_{z2}=\{\alpha_3\int_{C_1+C_3}A_{n\gamma}yds+(\alpha_1+\alpha_3)\int_{C_2+C_3}A_{n\gamma}yds\}/\Delta$$

$$f_{\phi 2}=\{\alpha_3\cdot 2A_I+(\alpha_1+\alpha_3)\cdot 2A_{II}\}/\Delta$$

$$f_{\omega 2}=-\{\alpha_3\int_{C_1+C_3}A_{n\gamma}\bar{\omega}ds+(\alpha_1+\alpha_3)\int_{C_2+C_3}A_{n\gamma}\bar{\omega}ds\}/\Delta$$

where

$$\Delta=\alpha_1\alpha_2+\alpha_2\alpha_3+\alpha_3\alpha_1 \quad \text{(a3)}$$

The α_i ($i=1, 3$) are defined in Eq. (14). The elements of the (5×5) stiffness matrix $[K_{bb}]$ in Eq. (17) are obtained by:

$$K_{bb}(1,1)=\oint A_{n\varepsilon}ds+\alpha_1f_{x1}^2+\alpha_2f_{x2}^2+\alpha_3(f_{x1}-f_{x2})^2$$

$$K_{bb}(1,2)=K_{bb}(2,1)=\oint A_{n\varepsilon}zds+\alpha_1f_{x1}f_{y1}+\alpha_2f_{x2}f_{y2}+\alpha_3(f_{x1}-f_{x2})(f_{y1}-f_{y2})$$

$$K_{bb}(1,3)=K_{bb}(3,1)=\oint A_{n\varepsilon}y_{ds}+\alpha_1f_{x1}f_{z1}+\alpha_2f_{x2}f_{z2}+\alpha_3(f_{x1}-f_{x2})(f_{z1}-f_{z2})$$

$$K_{bb}(1,4)=K_{bb}(4,1)=\alpha_1f_{x1}f_{\phi}+\alpha_2f_{x2}f_{\phi 2}+\alpha_3(f_{x1}-f_{x2})(f_{\phi 1}-f_{\phi 2})$$

$$K_{bb}(1,5)=K_{bb}(5,1)=\oint -A_{ns}\bar{\omega}ds+\alpha_1f_{x1}f_{\omega 1}+\alpha_2f_{x2}f_{\omega 2}+\alpha_3(f_{x1}-f_{x2})(f_{\omega 1}-f_{\omega 2})$$

$$K_{bb}(2,2)=\oint A_{n\varepsilon}z^2ds+\alpha_1f_{y1}^2+\alpha_2f_{y2}^2+\alpha_3(f_{y1}-f_{y2})^2$$

$$K_{bb}(2,3)=K_{bb}(3,2)=\oint A_{n\varepsilon}yzds+\alpha_1f_{y1}f_{z1}+\alpha_2f_{y2}f_{z2}+\alpha_3(f_{y1}-f_{y2})(f_{z1}-f_{z2})$$

$$K_{bb}(2,4)=K_{bb}(4,2)=\alpha_1f_{y1}f_{\phi 1}+\alpha_2f_{y2}f_{\phi 2}+\alpha_3(f_{y1}-f_{y2})(f_{\phi 1}-f_{\phi 2})$$

$$K_{bb}(2,5)=K_{bb}(5,2)=\oint -A_{n\varepsilon}\bar{\omega}zds+\alpha_1f_{y1}f_{\omega 1}+\alpha_2f_{y2}f_{\omega 2}+\alpha_3(f_{y1}-f_{y2})(f_{\omega 1}-f_{\omega 2})$$

$$K_{bb}(3,3)=\oint_{An\varepsilon}y^2ds+\alpha_1f_{z1}^2+\alpha_1f_{z2}^2+\alpha_3(f_{z1}-f_{z2})^2$$

$$K_{bb}(3,4)=K_{bb}(4,3)=\alpha_1f_{z1}f_{\phi 1}+\alpha_2f_{z2}f_{\phi 2}+\alpha_3(f_{z1}-f_{z2})(f_{\phi 1}-f_{\phi 2})$$

$$K_{bb}(3,5)=K_{bb}(5,3)=\oint -A_{n\varepsilon}\bar{\omega}yds+\alpha_1f_{z1}f_{\omega 1}+\alpha_2f_{z2}f_{\omega 2}+\alpha_3(f_{z1}-f_{z2})(f_{\omega 1}-f_{\omega 2})$$

$$K_{bb}(4,4)=\alpha_1f_{\phi 1}^2+\alpha_2f_{\phi 2}^2+\alpha_3(f_{\phi 1}-f_{\phi 2})^2$$

$$K_{bb}(4,5)=K_{bb}(5,4)=\alpha_1f_{\phi 1}f_{\omega 1}+\alpha_2f_{\phi 2}f_{\omega 2}+\alpha_3(f_{\phi 1}-f_{\phi 2})(f_{\omega 1}-f_{\omega 2})$$

$$K_{bb}(5,5)=\oint A_{n\varepsilon}\bar{\omega}^2ds+\alpha_1f_{\omega 1}^2+\alpha_2f_{\omega 2}^2+\alpha_3(f_{\omega 1}-f_{\omega 2})^2$$